Los Alamos, NM, 467-476 (1993)

AN EFFICIENT SYMPLECTIC APPROXIMATION FOR FRINGE–FIELD MAPS

G. H. Hoffstätter and M. Berz
Department of Physics and Astronomy, and
National Superconducting Cyclotron Laboratory
Michigan State University, East Lansing, MI 48824

ABSTRACT

The fringe fields of particle optical elements have a strong effect on optical properties. In particular higher order aberrations are often dominated by fringe-field effects. So far their transfer maps can only be calculated accurately using numerical integrators, which is rather time consuming. Any alternative or approximate calculation scheme should be symplectic because of the importance of the symplectic symmetry for long term behaviour. We introduce a method to approximate fringe-field maps of magnetic elements in a symplectic fashion which works extremely quickly and accurately. It is based on differential algebra (DA) techniques and was implemented in COSY INFINITY. The approximation exploits the advantages of Lie transformations, generating functions, scaling of the map with field strength and aperture, and the dependence of transfer maps on the ratio of magnetic rigidity to magnetic field strength. The results are compared to numerical integration and to the approximation via fringe-field integrals. The quality of the approximation will be illustrated on some examples including linear design, high order effects, and long term tracking.

INTRODUCTION

The fringe–field map of a static particle optical element is defined as the concatenation of an inverse drift from the effective field boundary to a point outside the field, the map through the fringe field, and the inverse map of the main field back to the effective field boundary[1,2,3]. This is illustrated in figure 1.

So far high order transfer maps of fringe fields can only be calculated accurately using numerical integrators[4], which is very time consuming. Figure 2 shows the ratio of the time used for the computation of the main–field map to the time used for the fringe–field maps of a typical quadrupole and dipole for different expansion orders. (The quadrupole used in the examples of this paper has: length 41.9cm, a pole–tip field of 2T, and an aperture of 2.54cm. The wedge dipole has radius 2m, an angle of 30°, and an aperture of 2.54cm. The ion chosen is $^{16}O^{3+}$ with an energy of 25MeV per nucleon. The fringe fields used are those of the Enge model[5,6,7].) The accurate consideration of fringe fields slows the computation down by orders of magnitude.

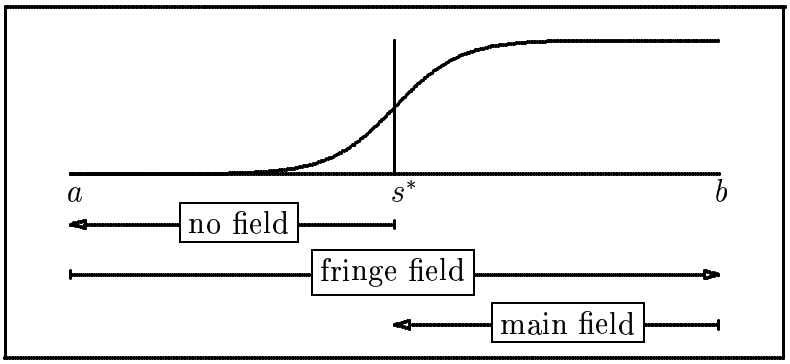

Figure 1: Definition of fringe–field maps.

The computation of main–field maps for multipoles is so speedy because no numerical integration is needed[8]. The map $\mathcal{M}(\vec{z})$ that transforms the canonical variables of motion $\vec{z}$ of a particle before the main field into those variables behind the main–field region can be calculated directly using the Lie derivative $L_f = \vec{f} \cdot \nabla + \partial_s$ that governs the motion $d\vec{z}/ds = \vec{f}(\vec{z})$ in the main field:

$$\frac{dg(\vec{z})}{ds} = L_f g(\vec{z}) \quad , \quad \mathcal{M}(\vec{z}) = e^{l_0 L_f} \vec{z} \tag{1}$$

where g is an differentiable function, s is the path length of the reference trajectory, and l_0 is the length of this trajectory in the main–field region. The first and second order is particularly fast since the equation of motion is evaluated analytically up to second order for multipoles. For dipoles, the equation of motion is solved analytically to all orders by geometrical reasoning, including edge angles and edge curvatures. Furthermore, the main–field map is accurate to machine precision (10^{-16}), whereas COSY uses a Runge–Kutta of eighth order which for the sake of speed is usually set to an accuracy of 10^{n-9} for order n. This integrator is thought to be most efficient for the differential equations of particle dynamics[9]. The righthand picture in figure 2 shows the normalized average relative difference for map coefficients computed with and without fringe fields for different orders of the map. Note especially that this average $< \frac{|a-b|}{|a|+|b|} > / \ln(2)$ would approach 1 for totally randomly distributed numbers a and b.

The simplest approximation is to ignore fringe fields, which is often referred to as the sharp cut off fringe field (SCOFF) approximation. This approximation is very inaccurate. Firstly, a field raising rapidly from zero to the main–field value does not satisfy Laplace's equation. In second order this problem was solved with the impulse approximation[10] which is used in the second–order particle optics code TRANSPORT and related codes[11]. Secondly, the detailed fringe–field shape has a strong effect on optical properties[1,2]. The results of computations with fringe

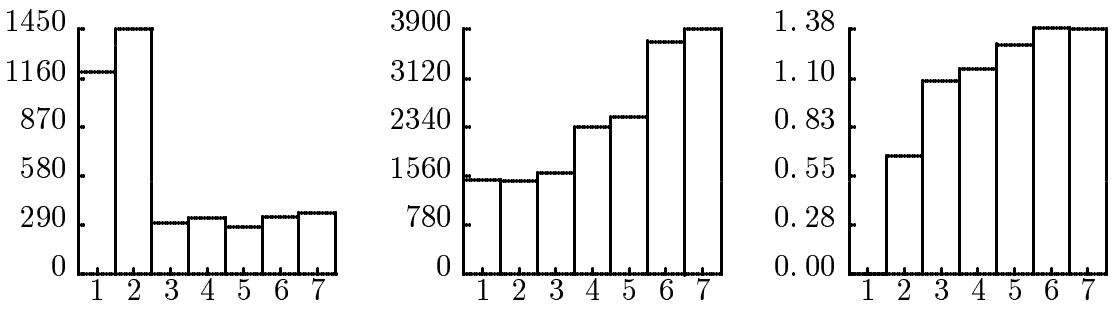

Figure 2: The ratio of computation speed for the two fringe–field maps and the main–field map using COSY INFINITY. Left: quadrupole, middle: dipole. Right: Average relative difference of map coefficients for a dipole with and without fringe field.

fields differ significantly from the results of the SCOFF approximation.

Often the effect of fringe fields is approximated by fringe–field integrals. This was done in third order for GIOS[12,13] and attempts are being made to extend this to fifth order for some particle optical elements[1,2]. The approximation by fringe–field integrals, however, has some serious disadvantages:

- It is nonsymplectic and therefore not especially suited for cases where symplectic tracking can be advantageous, for example circular machines.
- It represents the fringe effect well only if the region of the fringe field is not much bigger than the dimension of the beam diameter.
- It is limited to low orders and usually not very accurate.

In order to speed up the fringe–field calculation in the arbitrary order code COSY INFINITY, we searched for a method that does not have those drawbacks, works fast, and to all orders.

SYMPLECTIC SCALING

In the following we will use TRANSPORT notation for the map[14] which means the variables of motion are the cartesian coordinates and slopes x, x', y, y', the path length difference l, and the relative momentum deviation from a reference momentum δ_p. Those six quantities form the vector $\vec{z}$. The transfer map describes the transformation of an initial $\vec{z}_i$ into a final $\vec{z}_f$ by means of an optical element:

$$\vec{z}_f = \mathcal{M}^P(\vec{z}_i) \ . \tag{2}$$

The index P indicates that the map $\mathcal{M}$ depends on certain parameters like the momentum p, mass m, and charge z of the reference particle and the aperture A of the optical element.

From now on we will restrict ourselves to magnetostatic elements, although parts of the procedure are applicable to electrostatic elements, too. The bending radius of the path of a particle with momentum p at field B is

$$R = \frac{p}{zB_\perp} \tag{3}$$

where $B_\perp$ denotes the field component perpendicular to the momentum of the particle. All maps that describe particles with equivalent bending radii along their path are identical. If the map for a specific beam is known as a function of the field B at the pole tip, the transfer map for all other beams can be computed:

$$\mathcal{M}^{p^*,m^*,z^*,B^*} = \mathcal{M}^{p,m,z}(B)|_{B=B^*\frac{z^*p}{p^*z}} \ . \tag{4}$$

The map on the right hand side is known as a function of the field B, whereas the left hand side describes a map that is calculated at a certain field B^*. This is just another way of saying that the map depends only on the ratio of field to magnetic rigidity.

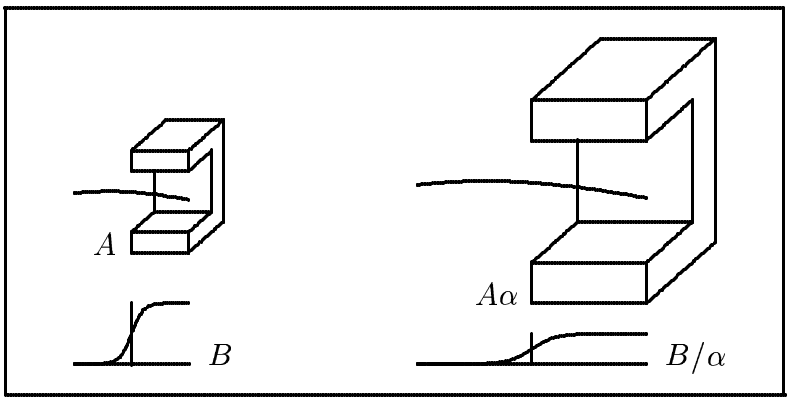

Figure 3: The coordinates of the particle trajectories in two elements scale with the factor α if the elements scale with the factor α and the fields scale with the factor $1/\alpha$.

Let us now consider two similar magnetostatic elements that differ only by a scaling factor α. If the bending radii also differ by a factor of α, the maps are similar. Equation (3) shows that this is the case whenever the increase in size by

a factor α is accompanied by a decrease in the field strength by the same factor. After scaling the coordinates x, y, l, we obtain

$$\left(\begin{array}{c} \mathcal{M}_{x}^{B/\alpha,A\alpha} \\ \mathcal{M}_{x'}^{B/\alpha,A\alpha} \\ \mathcal{M}_{l}^{B/\alpha,A\alpha} \\ \mathcal{M}_{\delta_p}^{B/\alpha,A\alpha} \end{array} \right)_{(x_i,x_i',l,\delta_p)} = \left(\begin{array}{c} \alpha\mathcal{M}_{x}^{B,A} \\ \mathcal{M}_{x'}^{B,A} \\ \alpha\mathcal{M}_{l}^{B,A} \\ \mathcal{M}_{\delta_p}^{B,A} \end{array} \right)_{(x_i/\alpha,x_i',l/\alpha,\delta_p)} . \tag{5}$$

The second dimension (y, y') is not mentioned because it has the same properties as (x, x').

To conclude, we state that the knowledge of the transfer map as a function of the field strength at the pole tip for particles with a specific magnetic rigidity and for an element with a specific aperture is sufficient to know all transfer maps of similar elements for all energies, masses, and charges. In fact the map does not even have to be known as a function of the field because the dependence on the field can be obtained by equation (4) from the dependence of the map on the momentum. In general it is useful and customary to work with the canonical coordinates[4] $(x, p_x/p_0, y, p_y/p_0, (t_0 - t)E_0/p_0, \delta_E)$ where the subscript 0 indicates quantities of the reference particle that defines the reference trajectory. For this purpose one has to transform between TRANSPORT and COSY notation.

COSY INFINITY can readily compute the map of a fringe field of certain aperture $\mathcal{M}^{E,m,z,A}$, with δ_E being the sixth variable. The map $\mathcal{M}^{E,m,z,A}$ of a certain fringe field for a certain beam has to be stored once as a function of B in order to compute maps of similar fields and all kind of beams. The functional dependence on B can be approximated by a Taylor expansion, the coefficients of which are computed by COSY INFINITY automatically. The accuracy of this expansion depends on the chosen order and on the relative difference of the ratio of bending radius to aperture in the scaled and the saved element. Unfortunately the symplectic structure of the map would not be conserved in this process. Symplecticity, however, is an intrinsic symmetry of canonical motion that arises from the special structure of Hamilton's equations. It should not be violated, especially when long term behaviour is of interest[15,16,17].

This drawback can be eliminated by storing the reference map $\mathcal{M}^{E,m,z,A}$ in a symplectic representation, either in the form of a generating function[18], or in the form of a Lie exponent

$$\vec{z}_f = L(B)e^{:P(B):}\vec{z}_i \ . \tag{6}$$

In higher orders the representation via generating functions is slow because a map inversion is required[8]. The Lie representation has the disadvantage that the matrix $L(B)$ can only be approximated and is not exactly symplectic. A combination of both methods is most efficient: We represent the nonlinear part by $P(B)$ and the

linear part by the generating function $F(B)$ that is most accurate for the given matrix $L(B)$.

EXAMPLES

In this section, we will illustrate the profitable use of the method with several examples. In order to evaluate speed and accuracy of the proposed approximation, we study a certain aberration coefficient of a quadrupole. Figure 4 shows the dependence of the expansion coefficient $(x|xxa)$ as a function of the field B at the pole tip. Because functions like this can be closely approximated by polynomials, symplectic scaling (SYSCA) is quite accurate. Even at the border of the

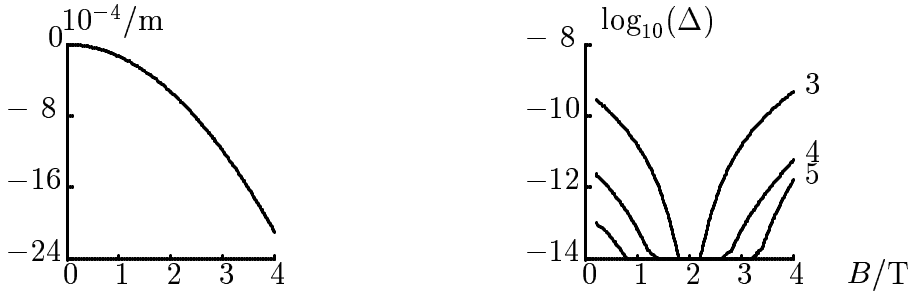

Figure 4: left: $(x|xxa)$ for a quadrupole as a function of the field at the pole tip. right: Error Δ of the approximation of $(x|xxa)$ with different expansion orders for the reference representation at B=2T.

range in figure 4 the presented method is more accurate than the COSY standard integrator. Close to the value with which the reference file was produced, the accuracy increases drastically. The results in figure 4 were obtained by evaluating the symplectic reference representation to third, fourth, and fifth order. The accuracy can be further improved by increasing this order which of course increases the computation time that has to be invested for creating the reference map in advance. This investment can be very much rewarding, especially when beamlines or spectrometers are being fitted or when system errors are analyzed so that maps of similar fringe fields are needed over and over again with only slightly different parameters. The SYSCA approximation is especially helpful in the design of a realistic system after approximate parameters of the elements have been obtained by neglecting fringe fields. These values can be used to create a reference file for symplectic scaling. In this way, a very high accuracy almost equivalent to accurate but time intensive numerical integration can be obtained. The time advantage of this method is illustrated in figure 5.

Fringe fields do have noticeable effects already in first order. In the example of the A1200[19] isotope separator at the NSCL, the effect of the fringe fields on

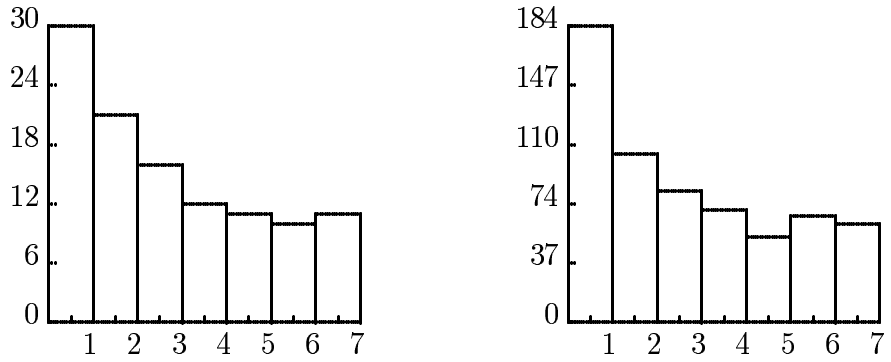

Figure 5: Factor of time advantage of SYSCA to numerical integration with accuracy of 10^{n-9} as a function of the expansion order. Left: Quadrupole, Right: Dipole.

Θ and C_0 with SCOFF approximation	80.8840°	−65.96m
Θ and C_0 with dipole fringe fields only	81.1696°	−65.96m
Θ and C_0 with quad fringe fields only	81.2694°	−682.68m
Θ and C_0 with SYSCA approximation	81.2701°	−687.10m
Θ and C_0 with actual fringe fields	81.2702°	−687.10m

Table 1: Tilt angle and opening aberration for various fringe–field models.

the calculated setting of the field strength is shown in figure 6. The fringe fields were described by Enge functions, and the Enge coefficients had been fitted to measured field data. Here the time advantage of the proposed approximation in the fit is three minutes versus two hours. As a measure of accuracy, we study the tilt angle Θ of the dispersive image plane and the opening aberration C_0 for various approximation methods. In the discussed device the coefficient $(x|aa)$ vanishes because of symmetry of the axial ray and anti symmetry of the dipole fields; therefore $(x|aaa)$ is the relevant opening aberration,

$$\Theta = -\frac{(x|a\delta)}{(a|a)(x|\delta)} \quad , \quad C_0 = (x|aaa) \ . \tag{7}$$

Table 1 shows Θ and C_o for various finge–field models. The values of Θ with and without fringe fields differ by 0.5% for the first dispersive image plane in the A1200; the third order aberration, however, is completely wrong if fringe fields are disregarded. This comparison also shows that quadrupole fringe fields, although often disregarded, can have effects which dominate over dipole fringe fields. Nonlinear effects can be seen by sending a cone of particles through the 7^{th} order A1200 map. The images with SCOFF and SYSCA approximation are shown in figure 7. The maximum angle used is 15mrad.

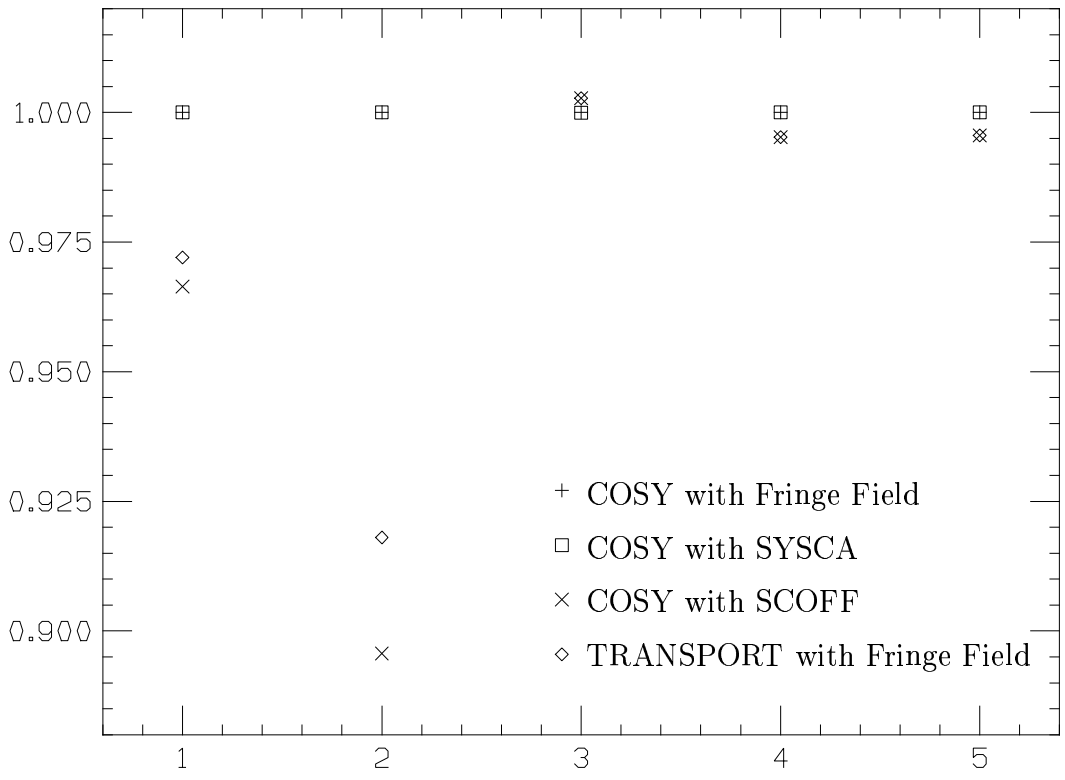

Figure 6: Relative deviation of predicted field settings with SCOFF and SYSCA from the correct settings for five quadrupoles. The standard fringe field approximation of TRANSPORT is given as a reference; the deviation is mainly due to the neglect of quadrupole fringe fields.

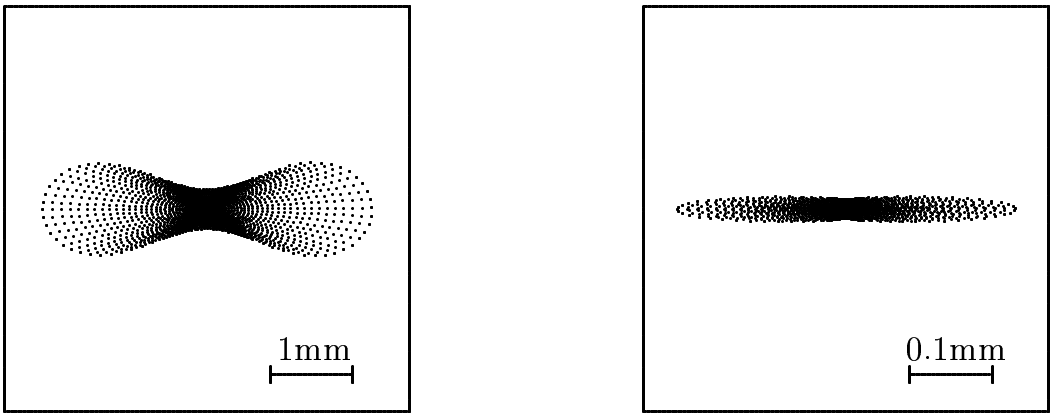

Figure 7: Beam spots with SYSCA (left) and SCOFF (right) approximation. The plot produced with the exact fringe fields can not be distinguished from the plot produced with SYSCA.

The effort involved in generating a symplectic approximation is rewarded when repetitive tracking is being performed. The example lattice of choice is the proposed PSR II Ring. The 9^{th} order 5000 turn tracking pictures are displayed in figure 8. The tracking was performed with the described standard numerical

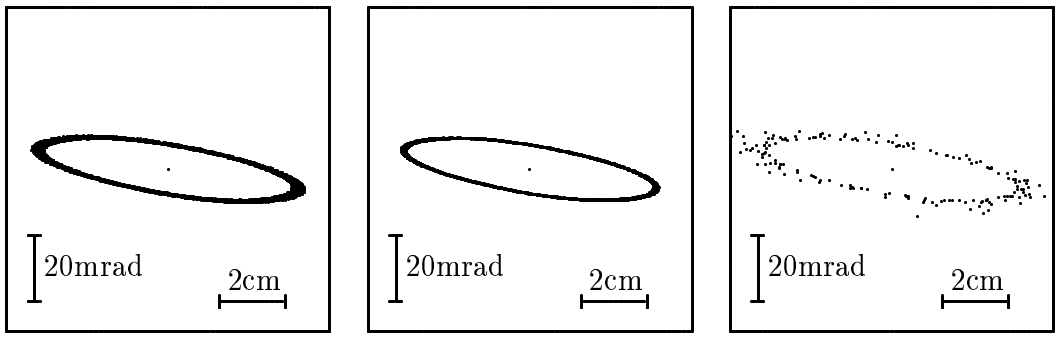

Figure 8: 5000 turn tracking with fringe fields obtained by numerical integration (left), SYSCA (middle), and a nonsymplectic fringe field approximation (right). The initial position of the particle is $(x, y) = (3\text{cm}, 3\text{cm})$ with no initial inclination.

integration, SYSCA, and a nonsymplectic fringe–field approximation obtained by low accuracy numerical integration. Nonsymplectic tracking rapidly destroys the phase space. SYSCA yields more stable results than the numerical integration since the limited accuracy of the numerical integrator slightly violates symplecticity. The corresponding 9^{th} order maps were produced with the SYSCA mode

in COSY INFINITY in 30 minutes, whereas the standard numerical integration took 15 hours, and the nonsymplectic approximation took 44 minutes on a VAX 4000–90 computer.

REFERENCE

1. B. Hartmann, M. Berz and H. Wollnik, Nucl. Instr. and Meth. A208, 343 (1990)
2. B. Hartmann, H. Irnich and H. Wollnik, Workshop on Nonlin. Effects in Accel. Phys., Berlin, IOP Publishing (1992)
3. H. Wollnik, Nucl. Instr. and Meth. 38, 56 (1965)
4. M. Berz, Nucl. Instr. and Meth. A298, 473 (1990)
5. M. Berz, COSY INFINITY User's Manual, MSUCL-869 (1993)
6. S. Kowalski and H. A. Enge, RAYTRACE User's Manual, Dept. of Physics MIT (1987)
7. K. L. Brown IEEE Transact. on Nucl. Science, NS-28, 3, 2568 (1981)
8. M. Berz, Nucl. Instr. and Meth. A298, 426 (1990)
9. Ingolf Kübler, Master's thesis, JLU Gießen, Germany (1987)
10. R. H. Helm, SLAC Technical Report 24 (1963)
11. R. Servranckx, private communication
12. H. Wollnik, B. Hartmann, and M. Berz, AIP Conference Proceedings, 177, 74 (1988)
13. H. Wollnik, GIOS User's Manual, JLU Gießen, Germany (1992)
14. K. L. Brown, F. Rothacker, D. C. Carey, and Ch. Iselin, TRANSPORT User's Manual, SLAC-91 (1977)
15. I. Gjaja, A. J. Dragt, D. T. Abell, Workshop on Nonlin. Effects in Accel. Phys., Berlin, IOP Publishing (1992)
16. R. Kleiss, F. Schmidt, Y. Yan, F. Zimmermann CERN SL/92-02
17. R. Kleiss, F Schmidt, F. Zimmermann CERN SL/92-31(AP)
18. H. Goldstein, Classical Mechanics (1980)
19. B. M. Sherrill et al. The First Intern. Conf. on Radioactive Nucl. Beams, Berkeley, World Scientific Publishing (1990)